Journal of Materials Chemistry A

COMMUNICATION

View Article Online
View Journal | View Issue

Cite this: J. Mater. Chem. A, 2017, 5, 17204

Received 5th July 2017
Accepted 26th July 2017

DOI: 10.1039/c7ta05809h

rsc.li/materials-a

New small-molecule acceptors based on hexacyclic naphthalene(cyclopentadithiophene) for efficient non-fullerene organic solar cells†

Yuan-Qiu-Qiang Yi, ‡ Huanran Feng,‡ Meijia Chang, Hongtao Zhang,* Xiangjian Wan, Chenxi Li and Yongsheng Chen *

A series of new non-fullerene small molecule acceptors (**NTIC**, **NTIC-Me**, **NTIC-OMe** and **NTIC-F**) based on the acceptor–donor–acceptor (A–D–A) architecture, using hexacyclic naphthalene-(cyclopentadithiophene) as the central unit, were designed and synthesized. The non-fullerene OSC device based on PBDB-T:**NTIC** showed a highest PCE of 8.63%. With a relatively high-lying LUMO level of **NTIC-OMe**, the PBDB-T:**NTIC-OMe** based device obtained a comparatively high V_{oc} of 0.965 V and a PCE of 8.61% simultaneously. The results demonstrate that the naphthalene core is a promising building block for constructing highly efficient non-fullerene acceptors and further boosting the photovoltaic performance of the devices.

Introduction

Organic solar cells (OSCs) are one of the most promising technologies for solar energy conversion due to their attractive advantages such as low cost, light weight, mechanical flexibility and solution processibility.[1–3] Over the last decade, thanks to the dramatic development of donor materials, including polymers and small molecules, as well as device optimization, fullerene-based OSCs have gained power conversion efficiencies (PCEs) greater than 12%.[4–10] Fullerene derivatives ($PC_{61}BM$ and $PC_{71}BM$) have been widely used as acceptor materials, partially due to their high electron affinity and electron mobility, isotropic charge transportation, and formation of appropriate phase separation.[11,12] In spite of the great success achieved by fullerene-based OSCs, the intrinsic drawbacks, such as their weak absorption of visible light, poor chemical and electronic adjustability, are the constraints for further improving the photovoltaic performance of OSCs. To tackle these issues, great attentions have been paid to develop non-fullerene acceptors with highly efficient absorption, facile synthesis and easily tuned energy levels.[13–16]

From the perspective of molecule design, the strategy of the incorporation of π-fused conjugated moieties, such as perylene diimide (PDI), naphthalene diimide (NDI), fluoranthene-fused diimide, and diketopyrrolopyrrole (DPP), has been widely explored.[17–27] For small molecules, the successful donor materials are mostly with backbone structures of acceptor–donor–acceptor (A–D–A) and have been widely used in highly efficient fullerene-based OSCs.[28–32] Similarly, small-molecule acceptors with the A–D–A architecture have drawn great attention towards constructing devices with high efficiency.[33–36] So far, the performance of non-fullerene (NF) based OSCs has surpassed those of fullerene-based opponents.[37–41] Zhan *et al.* reported some pioneering A–D–A type NF small-molecule acceptors using an extended fused-ring indacenodithiophene (IDT) or indacenodithieno[3,2-*b*]thiophene (IDTT) as central building blocks, such as IDIC, ITIC and ITIC-Th. Recently, a series of NF small-molecule acceptors ITIC and their analogues have been synthesized, and excellent photovoltaic performance has been achieved for the devices using these materials.[42–47]

Recently, we reported two NF small-molecule acceptors FDICTF and NFBDT for highly efficient OSCs,[48,49] in which the π-extended donor cores are fluorenedicyclopentathiophene and heptacyclic benzodi(cyclopentadithiophene), respectively. Since these two NF small-molecule acceptors have good light absorptions and high and balanced charge mobilities in blend films, they exhibited excellent photovoltaic performances with PCEs over 10%. In A–D–A type NF acceptors, planar π-extended donor cores could deliver red-shifted absorptions for harvested photons and enhanced J_{sc}. Thus, the strategy of using the ladder-type fused π-extended ring as a core unit should be a wise choice for constructing highly efficient NF OSCs.

Here, we report a new series of ladder type NF small-molecule acceptors with the A–D–A architecture utilizing hexacyclic naphthalene(cyclopentadithiophene) as the core unit and 2-

The Centre of Nanoscale Science and Technology, Key Laboratory of Functional Polymer Materials, State Key Laboratory and Institute of Elemento-Organic Chemistry, Collaborative Innovation Center of Chemical Science and Engineering (Tianjin), College of Chemistry, Nankai University, Tianjin, 300071, China. E-mail: htzhang@nankai.edu.cn; yschen99@nankai.edu.cn

† Electronic supplementary information (ESI) available. See DOI: 10.1039/c7ta05809h

‡ Yuan-Qiu-Qiang Yi and Huanran Feng contributed equally to this work.

(2,3-dihydro-3-oxo-1*H*-inden-1-ylidene)propanedinitrile (INCN) as the end group, named **NTIC**. The fused naphthalene(cyclopentadithiophene) core unit has good planarity and rigidity because it is covalently bridged by the sp^3-carbon with an alkyl phenyl group as the side chain. The resulting planar backbones could guarantee **NTIC** avoiding strong aggregation in the solid state to meet the requirements for efficient OSCs, such as good absorption, high mobility, and ideal morphology in the photoactive layer. We synthesized four non-fullerene small molecule acceptors as depicted in Scheme 1, namely **NTIC**, **NTIC-Me**, **NTIC-OMe** and **NTIC-F**, with different substitutes on the end group. With this, we systematically investigated the substitution effect of end groups on the morphology of the BHJ layer and the photovoltaic performance of NF OSCs. From the perspective of complementary absorptions and energy levels, a wide band gap polymer poly[(2,6-(4,8-bis(5-(2-ethylhexyl)thiophen-2-yl)-benzo[1,2-*b*:4,5-*b*′]dithiophene))-*alt*-(5,5-(1′,3′-di-2-thienyl-5′,7′-bis(2-ethylhexyl)benzo[1′,2′-*c*:4′,5′-*c*′]-dithiophene-4,8-dione))] (PBDB-T) was selected as the donor material to fabricate devices with **NTIC** and its analogues as the electron acceptor materials. The highest PCE of 8.63% could be obtained by the device based on PBDB-T:**NTIC**. The device based on PBDB-T:**NTIC-OMe** could deliver a PCE of 8.61%, while in the meantime, a comparatively high V_{oc} of 0.965 V could still be obtained.

Results and discussion

Material synthesis and thermal properties

The synthetic route for **NTIC** is depicted in Scheme 1. The Suzuki coupling reaction between compound **1** and ethyl 2-bromo-3-thiophenecarboxylate could deliver compound **2** in a yield of 88%. Compound **2** was nucleophilically attacked by excess aryl lithium reagents to get the tertiary alcohol, which could be used in the next step without purification. The intramolecular Friedel–Crafts reaction of the tertiary alcohol was catalysed by trifluoromethanesulfonic acid and gave the π-fused ring core **3**. The dialdehyde compound **4** was prepared by the Vilsmeier–Haack reaction with $POCl_3$ and DMF (*N*,*N*-dimethylformamide) as a light-yellow solid. The desired **NTIC** was then obtained by the Knoevenagel condensation of the dialdehyde compound **4** with INCN in a good yield. **NTIC-Me**, **NTIC-OMe** and **NTIC-F** were synthesized by a similar procedure using different substituted INCN. **NTIC**, **NTIC-Me**, **NTIC-OMe** and **NTIC-F** were fully characterized by ^{1}H NMR, ^{13}C NMR, and matrix assisted laser desorption ionization time of flight mass spectrometry (MALDI-TOFMS). All the non-fullerene acceptors exhibit good solubility in common solvents (such as dichloromethane, chloroform and chlorobenzene). The thermal properties of the four compounds were measured by thermogravimetric analysis (TGA), and the data are shown in Table 1 and Fig. S1.† They all show good thermal stability with the decomposition temperature (5% weight loss) over 340 °C under a nitrogen atmosphere. From the curves of the differential scanning calorimetry (DSC) in Fig. S2,† no obvious melting point or recrystallization point was observed.

Photophysical and electrochemical properties

The photophysical properties of **NTIC**, **NTIC-Me**, **NTIC-OMe** and **NTIC-F** in $CHCl_3$ solution and as thin films were investigated by UV-vis absorption spectroscopy and are depicted in Fig. S5† and 1d, respectively. These four molecules in diluted chloroform solution exhibit strong and broad absorption in the region of 500–700 nm, which is complementary to that of PBDB-T. **NTIC**, **NTIC-Me**, **NTIC-OMe** and **NTIC-F** in $CHCl_3$ solution showed an absorption peak at 650, 646, 651 and 657 nm, respectively, and the maximum molar extinction coefficients were determined to be 6.8×10^4, 8.5×10^4, 1.1×10^5 and 7.2×10^4 M^{-1} cm^{-1}, respectively. **NTIC**, **NTIC-Me** and **NTIC-OMe** films showed a red-shifted absorption peak at 694, 670 and 675 nm, respectively, while the **NTIC-F** film shows a more bathochromic-shift of 56 nm compared with that of its solution, indicating a more-ordered structure and closer π–π stacking in the thin film. The electrochemical behaviour of **NTIC**, **NTIC-Me**,

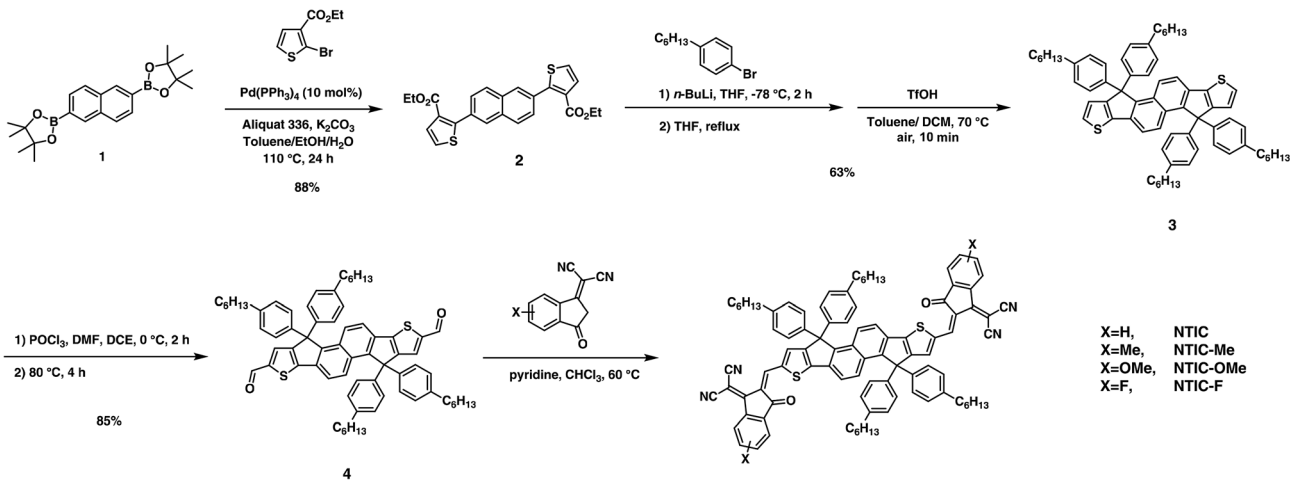

Scheme 1 The synthetic routes to NTIC, NTIC-Me, NTIC-OMe and NTIC-F.

Table 1 Physical, optical and electrochemical data

Acceptors	T_d[a] (°C)	λ_{max}^{sol} (nm)	λ_{max}^{film} (nm)	λ_{edge}^{film}[b] (nm)	E_g^{optc} (eV)	LUMO (eV)	HOMO (eV)	E_g^{CV} (eV)
NTIC	343	650	694	741	1.67	−3.76	−5.58	1.82
NTIC-Me	356	647	670	711	1.74	−3.73	−5.53	1.80
NTIC-OMe	376	651	675	726	1.71	−3.70	−5.53	1.83
NTIC-F	344	657	712	748	1.66	−3.77	−5.52	1.75

[a] T_d is the temperature at 5% weight-loss under a N_2 atmosphere. [b] Calculated from the onset absorption of **NTIC**, **NTIC-Me**, **NTIC-OMe** and **NTIC-F**. [c] $E_g^{opt} = 1240/\lambda_{edge}$.

NTIC-OMe and **NTIC-F** was investigated by cyclic voltammetry (CV) in dichloromethane solution. The energy levels were estimated from the oxidation and reduction curve in CV spectra, and the measurement was referenced to the energy level of Fc/Fc^+ (−4.8 eV below the vacuum level). The electrochemical and optical data are listed in Table 1. The LUMO levels of **NTIC-Me** and **NTIC-OMe** are estimated to be −3.73 eV and −3.70 eV, respectively, which are 0.03 and 0.06 eV higher than that of **NTIC** (−3.76 eV). In contrast to these typical electron acceptors, the comparatively high-lying LUMO levels of **NTIC**, **NTIC-Me** and **NTIC-OMe** indicate that a higher V_{oc} could be obtained when used in non-fullerene OSCs. In addition, the LUMO offsets between PBDB-T and these four acceptors (**NTIC**, **NTIC-Me**, **NTIC-OMe** and **NTIC-F**) are all larger than 0.7 eV, which are sufficient enough to transfer electrons from PBDB-T to the NF acceptor.

The photoluminescence (PL) spectra of the pure donor/acceptor and the blend films were measured, and the results are shown in Fig. S3.† Compared with the neat film of NF acceptors (**NTIC**, **NTIC-Me**, **NTIC-OMe** and **NTIC-F**), each blend film of the donor/acceptor exhibits significant fluorescence quenching, indicating that effective photo-induced charge transport occurs between PBDB-T and acceptors in the blend films, and almost all excitons dissociate, which is a prerequisite for efficient photovoltaic performance.

Photovoltaic properties

To evaluate the photovoltaic properties of the four new non-fullerene acceptors, conventional OSCs based on PBDB-T:acceptor (**NTIC**, **NTIC-Me**, **NTIC-OMe** and **NTIC-F**, respectively) were fabricated with a device structure of ITO (indium tin oxide)/PEDOT:PSS (poly(3,4-ethylenedioxythiopene):poly-(styrenesulfonate))/active layer/PDINO (*N*,*N*′-bis(propylenedi-methylamine)-3,4:9,10-perylenediimide)/Al, where PDINO, developed by Li,[50] is an effective cathode interlayer for efficient charge extraction and reducing recombination losses. After a series of optimization

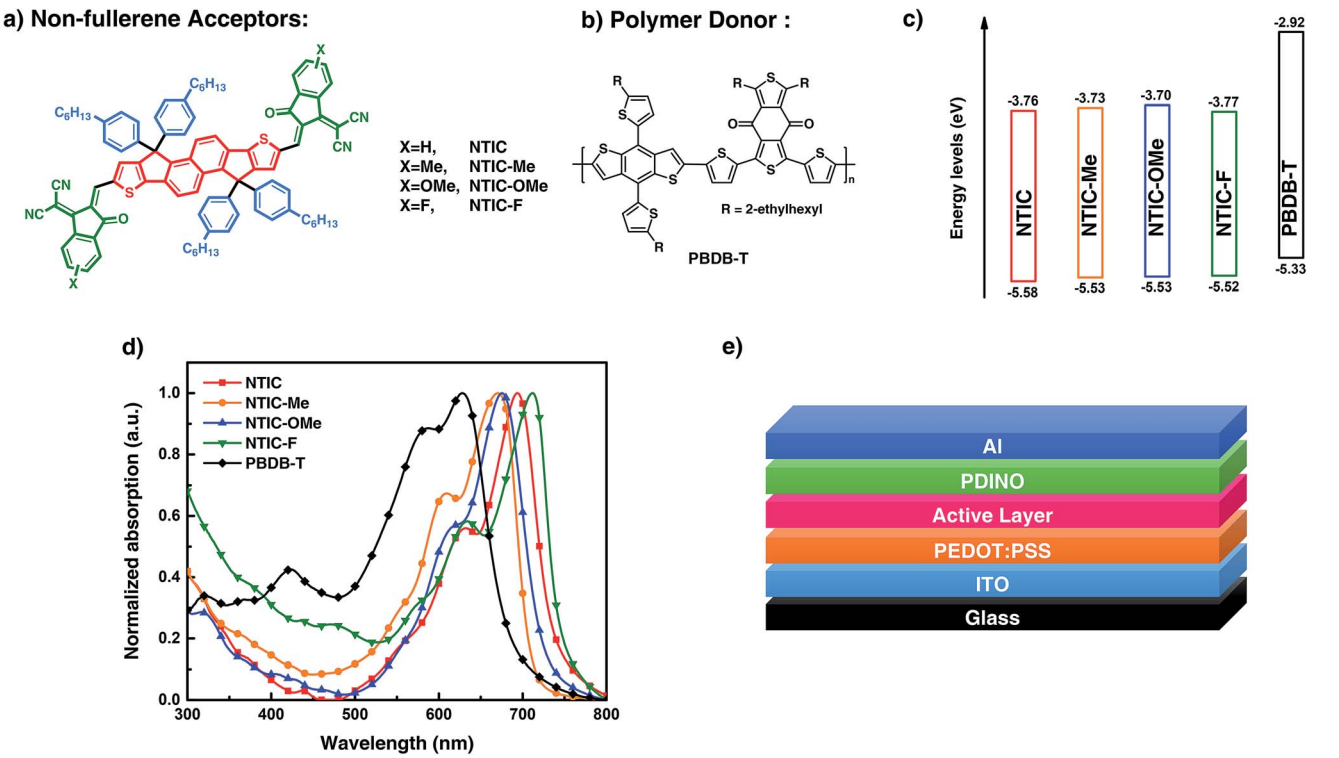

Fig. 1 (a) Chemical structures of NTIC, NTIC-Me, NTIC-OMe and NTIC-F. (b) Chemical structure of PBDB-T. (c) Energy levels of the donor and acceptors. (d) UV-vis absorption spectra of the as-cast film of the donor and acceptors. (e) The device structure.

(Table 2), by using chloroform as the processing solvent, the optimal D/A weight ratio for all blends is 1 : 0.8, and the thickness of the active layer is about 100 nm. OSC devices based on the as-cast PBDB-T:**NTIC**/**NTIC-Me**/**NTIC-OMe**/**NTIC-F** films showed PCEs of 7.43%, 7.80%, 8.12% and 6.50%, respectively. With further chloroform solvent vapour annealing treatment, the PCEs of the four devices increased to 8.63%, 8.30%, 8.61% and 8.10%, respectively. Benefitting from the relatively high-lying LUMO energy levels of **NTIC**, **NTIC-Me** and **NTIC-OMe**, these three devices obtained a comparatively high V_{oc} of 0.935, 0.963 and 0.965 V, respectively. Since **NTIC-F** has more red-shifted UV-vis spectra absorption, the device based on **NTIC-F** gave a relatively higher J_{sc} of 15.04 mA cm^{-2} compared with the other three devices. The current-density–voltage (J–V) curves of the OSCs based on PBDB-T:**NTIC**/**NTIC-Me**/**NTIC-OMe**/**NTIC-F** with the optimal photovoltaic performance are summarized in Fig. 2a, and the corresponding photovoltaic parameters are listed in Table 2.

The EQE spectra of devices with SVA are depicted in Fig. 2b. As indicated by the complementary UV-vis absorption of acceptors and the donor shown in Fig. 1d, the broad and high EQE curves ranging from 300 nm to 720 nm indicate that both polymer donor PBDB-T and NF acceptors made a separate and complementary contribution to the overall J_{sc} values. The EQE values of all the devices with SVA were higher than those of the as-cast ones, which is indicative of high photoelectron conversion efficiency in the devices with SVA treatment. The device based on PBDB-T:**NTIC-F** with SVA reached a highest EQE value of 74% and over 70% from 560 to 720 nm, while the other three devices gave relatively lower EQE values. This could be ascribed to their blue-shifted absorption spectra.

The plots of photocurrent (J_{ph}) *versus* the effective applied voltage (V_{eff}) for the four devices with SVA were measured to investigate the exciton dissociation and charge collection properties in the devices (Fig. 2c). $J_{ph} = J_L - J_D$, where J_L is the current density under illumination and J_D is the current density in the dark. $V_{eff} = V_o - V_a$, where V_a is the applied voltage and V_o is the voltage at which J_{ph} is zero.[51] As depicted in Fig. 2c, when V_{eff} reaches ~2 V, J_{ph} values for all the four devices reach saturation (J_{sat}), suggesting that charge recombination is minimized at higher voltage due to the high internal electric field in the devices. The charge dissociation and charge collection probability ($P(E, T)$) in the devices could be estimated by calculating the value of J_{ph}/J_{sat}.[52] Under the conditions of the short-circuit and the maximal power output, $P(E, T)$ values are 95%, 78% for the **NTIC** based device, 92%, 74% for the **NTIC-Me** based device, 95%, 78% for the **NTIC-OMe** based device and 94%, 80% for the **NTIC-F** based device, respectively. The higher $P(E, T)$ values of **NTIC** and **NTIC-OMe** based devices indicate that these two devices exhibit higher exciton dissociation and more efficient charge collection efficiency compared to the other devices.

The light-intensity (P) dependence of J_{sc} was measured to further investigate the charge recombination properties in the devices (Fig. 2d). The relationship between J_{sc} and P can be described by the power-law equation $J_{sc} \propto P^{\alpha}$, where the power-law exponent α implies the extent of bimolecular recombination. As can be seen in Fig. 2d, the α value for the device based on PBDB-T:**NTIC**, PBDB-T:**NTIC-Me**, PBDB-T:**NTIC-OMe** and PBDB-T:**NTIC-F** is 0.96, 0.96, 0.94 and 0.96, respectively. This indicates that small bimolecular recombination occurred in the devices based on this series of non-fullerene acceptors.

Morphology characterization and charge transport

The morphology of the active layers was studied by the atomic force microscopy (AFM) in the tapping mode and transmission electron microscopy (TEM). As can be seen in the AFM images in Fig. 3a–d, the root-mean-square roughness of the SVA-treated blend films of PBDB-T:**NTIC**/**NTIC-Me**/**NTIC-OMe**/**NTIC-F** gave low values of 1.30, 1.80, 1.99 and 1.50 nm, respectively. The TEM images of the four optimized blend films are showed in Fig. 3e–h. All the blend films are uniform and without large phase separation. Among all the blend films, the PDBD-T:**NTIC** and PDBD-T:**NTIC-OMe** films exhibited increased nanofibrils and the more desired bi-continuous interpenetrating network between the donor and the acceptor, benefitting charge carrier generation and transportation. The bulk charge transport properties of the blend films with SVA were measured by the space-charge limited current (SCLC) method. The hole and electron mobilities were measured with device structures of ITO/PEDOT:PSS/active layer/Au and Al/active layer/Al. The PBDB-T:**NTIC**, PBDB-T:**NTIC-Me**, PBDB-T:**NTIC-OMe** and PBDB-T:**NTIC-F** photoactive layers showed

Table 2 Device parameters of OSCs based on PBDB-T and four acceptors under the illumination of AM 1.5G, 100 mW cm^{-2}

			J_{sc} (mA cm^{-2})			PCE (%)	
Acceptors	Treatment	V_{oc} (V)	Experiment	Calculated	FF (%)	Best	Average[a]
NTIC	As-cast	0.926	13.19		60.8	7.43	7.31
	SVA	0.935	13.55	12.98	68.1	8.63	8.50
NTIC-Me	As-cast	0.961	12.50		64.9	7.80	7.58
	SVA	0.963	13.03	12.48	66.2	8.30	8.12
NTIC-OMe	As-cast	0.962	12.97		65.1	8.12	8.03
	SVA	0.965	13.52	12.74	66.0	8.61	8.47
NTIC-F	As-cast	0.811	13.61		58.9	6.50	6.22
	SVA	0.812	15.04	14.62	66.3	8.10	7.97

[a] The average PCEs are based on twenty devices.

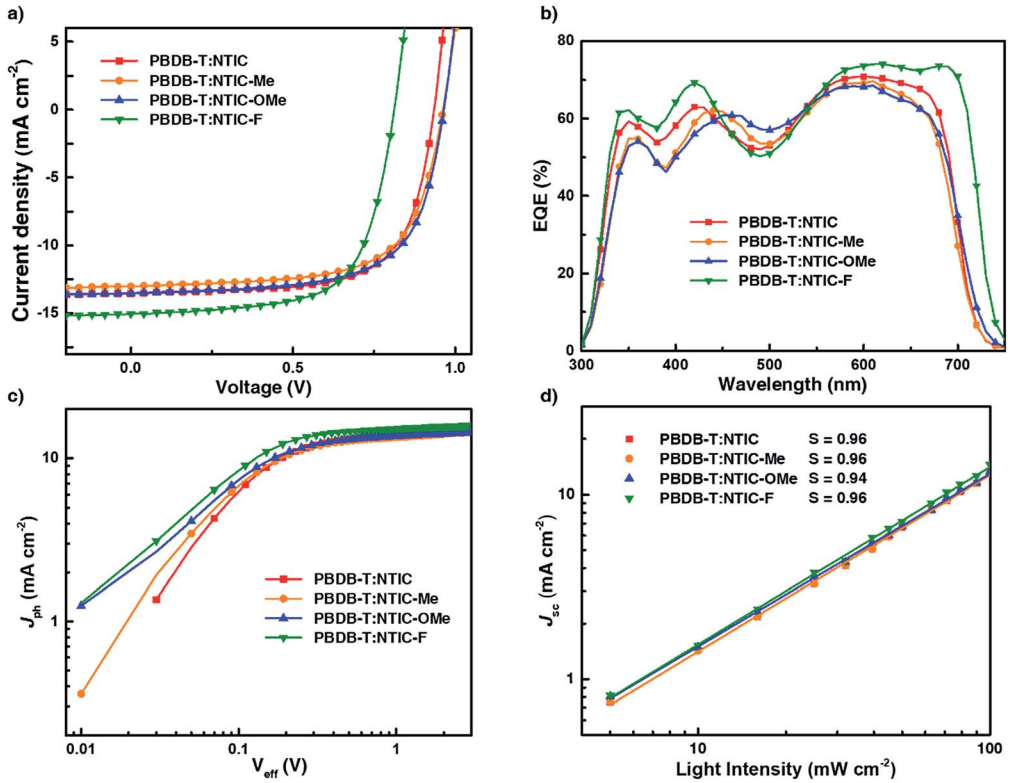

Fig. 2 (a) J–V and (b) EQE curves based on the devices with SVA. (c) J_{ph} *versus* V_{eff} and (d) light-intensity dependence of J_{sc} of the corresponding devices.

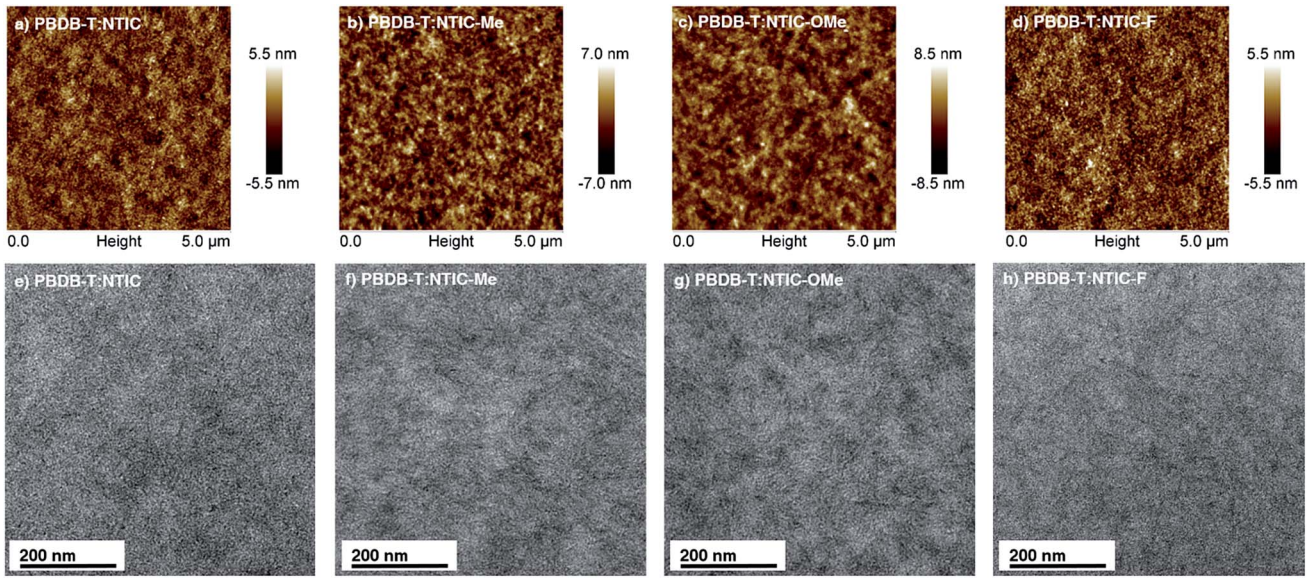

Fig. 3 (a–d) AFM images of the blend films with SVA. (e–h) TEM images of the blend films with SVA.

a hole/electron mobility of $19.1 \times 10^{-5}/9.15 \times 10^{-5}$ cm^{-2} V^{-1} s^{-1}, $7.29 \times 10^{-5}/6.93 \times 10^{-5}$ cm^{-2} V^{-1} s^{-1}, $8.49 \times 10^{-5}/7.86 \times 10^{-5}$ cm^{-2} V^{-1} s^{-1} and $8.00 \times 10^{-5}/6.59 \times 10^{-5}$ cm^{-2} V^{-1} s^{-1}, respectively. The comparatively higher hole and electron mobilities of the PBDB-T:**NTIC** blend film lead to an enhanced FF and the best PCE of the devices.

Conclusions

In summary, we have designed and synthesized a new series of acceptor–donor–acceptor (A–D–A) type non-fullerene acceptors with the ladder type fused ring using naphthalene as the central unit. Through the modification of substituents (H, Me, OMe

and F) on the end group, a highest PCE of 8.63% was achieved in the OSC device based on PBDB-T:**NTIC**. Due to the high-lying LUMO levels of **NTIC**, **NTIC-Me** and **NTIC-OMe**, the OSC devices fabricated with PBDB-T as the donor showed relatively high V_{oc} of up to 0.935, 0.963 and 0.965 V, respectively, which could be further used as the front cell in the tandem device in the near future. Therefore, the incorporation of the naphthalene core into an A–D–A backbone structure is an effective strategy for designing non-fullerene acceptors for high performance OSCs. With the versatile chemical structure of naphthalene, NF-acceptors based on the naphthalene core have great potential to be designed and modified for screening highly efficient OSCs.

Acknowledgements

The authors gratefully acknowledge the financial support from the Ministry of Science and Technology of China (MoST) (2014CB643502 and 2016YFA0200200) and NSFC (91433101, 51422304 and 51373078).

Notes and references

1 G. Yu, J. Gao, J. C. Hummelen, F. Wudl and A. J. Heeger, *Science*, 1995, **270**, 1789.
2 R. F. Service, *Science*, 2011, **332**, 293.
3 G. Li, R. Zhu and Y. Yang, *Nat. Photonics*, 2012, **6**, 153.
4 Y. Liu, J. Zhao, Z. Li, C. Mu, W. Ma, H. Hu, K. Jiang, H. Lin, H. Ade and H. Yan, *Nat. Commun.*, 2014, **5**, 5293.
5 B. Kan, M. Li, Q. Zhang, F. Liu, X. Wan, Y. Wang, W. Ni, G. Long, X. Yang, H. Feng, Y. Zuo, M. Zhang, F. Huang, Y. Cao, T. P. Russell and Y. Chen, *J. Am. Chem. Soc.*, 2015, **137**, 3886.
6 V. Vohra, K. Kawashima, T. Kakara, T. Koganezawa, I. Osaka, K. Takimiya and H. Murata, *Nat. Photonics*, 2015, **9**, 403.
7 L. Nian, K. Gao, F. Liu, Y. Kan, X. Jiang, L. Liu, Z. Xie, X. Peng, T. P. Russell and Y. Ma, *Adv. Mater.*, 2016, **28**, 8184.
8 Y. Jin, Z. Chen, S. Dong, N. Zheng, L. Ying, X. F. Jiang, F. Liu, F. Huang and Y. Cao, *Adv. Mater.*, 2016, **28**, 9811.
9 P. Fu, X. Guo, B. Zhang, T. Chen, W. Qin, Y. Ye, J. H. Hou, J. Zhang and C. Li, *J. Mater. Chem. A*, 2016, **4**, 16824.
10 Q. Wan, X. Guo, Z. Y. Wang, W. B. Li, B. Guo, W. Ma, M. J. Zhang and Y. F. Li, *Adv. Funct. Mater.*, 2016, **26**, 6635.
11 L. Lu, T. Zheng, Q. Wu, A. M. Schneider, D. Zhao and L. Yu, *Chem. Rev.*, 2015, **115**, 12666.
12 O. Ostroverkhova, *Chem. Rev.*, 2016, **116**, 13279.
13 Y. Lin, Y. Li and X. Zhan, *Chem. Soc. Rev.*, 2012, **41**, 4245.
14 C. B. Nielsen, S. Holliday, H. Y. Chen, S. J. Cryer and I. McCulloch, *Acc. Chem. Res.*, 2015, **48**, 2803.
15 Y. Z. Lin and X. W. Zhan, *Adv. Energy Mater.*, 2015, **5**, 1501063.
16 S. M. McAfee, J. M. Topple, I. G. Hill and G. C. Welch, *J. Mater. Chem. A*, 2015, **3**, 16393.
17 Q. Wu, D. Zhao, A. M. Schneider, W. Chen and L. Yu, *J. Am. Chem. Soc.*, 2016, **138**, 7248.
18 K. Gao, L. Li, T. Lai, L. Xiao, Y. Huang, F. Huang, J. Peng, Y. Cao, F. Liu, T. P. Russell, R. A. Janssen and X. Peng, *J. Am. Chem. Soc.*, 2015, **137**, 7282.
19 A. Tang, C. Zhan, J. Yao and E. Zhou, *Adv. Mater.*, 2017, **29**, 1600013.
20 Y. Zhong, M. T. Trinh, R. Chen, W. Wang, P. P. Khlyabich, B. Kumar, Q. Xu, C. Y. Nam, M. Y. Sfeir, C. Black, M. L. Steigerwald, Y. L. Loo, S. Xiao, F. Ng, X. Y. Zhu and C. Nuckolls, *J. Am. Chem. Soc.*, 2014, **136**, 15215.
21 J. W. Jung, J. W. Jo, C. C. Chueh, F. Liu, W. H. Jo, T. P. Russell and A. K. Jen, *Adv. Mater.*, 2015, **27**, 3310.
22 W. Ni, M. Li, B. Kan, F. Liu, X. Wan, Q. Zhang, H. Zhang, T. P. Russell and Y. Chen, *Chem. Commun.*, 2016, **52**, 465.
23 Y. J. Hwang, H. Li, B. A. Courtright, S. Subramaniyan and S. A. Jenekhe, *Adv. Mater.*, 2016, **28**, 124.
24 Y. J. Hwang, T. Earmme, B. A. Courtright, F. N. Eberle and S. A. Jenekhe, *J. Am. Chem. Soc.*, 2015, **137**, 4424.
25 F. Fernandez-Lazaro, N. Zink-Lorre and A. Sastre-Santos, *J. Mater. Chem. A*, 2016, **4**, 9336.
26 M. M. Li, Y. T. Liu, W. Ni, F. Liu, H. R. Feng, Y. M. Zhang, T. T. Liu, H. T. Zhang, X. J. Wan, B. Kan, Q. Zhang, T. P. Russell and Y. S. Chen, *J. Mater. Chem. A*, 2016, **4**, 10409.
27 D. Meng, H. Fu, C. Xiao, X. Meng, T. Winands, W. Ma, W. Wei, B. Fan, L. Huo, N. L. Doltsinis, Y. Li, Y. Sun and Z. Wang, *J. Am. Chem. Soc.*, 2016, **138**, 10184.
28 Y. Chen, X. Wan and G. Long, *Acc. Chem. Res.*, 2013, **46**, 2645.
29 W. Ni, M. Li, X. Wan, Y. Zuo, B. Kan, H. Feng, Q. Zhang and Y. Chen, *Sci. China: Chem.*, 2014, **58**, 339.
30 Y. Q. Guo, Y. C. Wang, L. C. Song, F. Liu, X. J. Wan, H. T. Zhang and Y. Chen, *Chem. Mater.*, 2017, **29**, 3694.
31 Q. Zhang, B. Kan, F. Liu, G. Long, X. Wan, X. Chen, Y. Zuo, W. Ni, H. Zhang, M. Li, Z. Hu, F. Huang, Y. Cao, Z. Liang, M. Zhang, T. P. Russell and Y. Chen, *Nat. Photonics*, 2014, **9**, 35.
32 B. Kan, Q. Zhang, M. Li, X. Wan, W. Ni, G. Long, Y. Wang, X. Yang, H. Feng and Y. Chen, *J. Am. Chem. Soc.*, 2014, **136**, 15529.
33 W. Zhao, D. Qian, S. Zhang, S. Li, O. Inganas, F. Gao and J. Hou, *Adv. Mater.*, 2016, **28**, 4734.
34 S. Holliday, R. S. Ashraf, A. Wadsworth, D. Baran, S. A. Yousaf, C. B. Nielsen, C. H. Tan, S. D. Dimitrov, Z. Shang, N. Gasparini, M. Alamoudi, F. Laquai, C. J. Brabec, A. Salleo, J. R. Durrant and I. McCulloch, *Nat. Commun.*, 2016, **7**, 11585.
35 H. Zhang, Y. Liu, Y. Sun, M. Li, W. Ni, Q. Zhang, X. Wan and Y. Chen, *Sci. China: Chem.*, 2016, **60**, 366.
36 F. Liu, Z. Zhou, C. Zhang, T. Vergote, H. Fan, F. Liu and X. Zhu, *J. Am. Chem. Soc.*, 2016, **138**, 15523.
37 S. Li, L. Ye, W. Zhao, S. Zhang, S. Mukherjee, H. Ade and J. Hou, *Adv. Mater.*, 2016, **28**, 9423.
38 J. Liu, S. S. Chen, D. P. Qian, B. Gautam, G. F. Yang, J. B. Zhao, J. Bergqvist, F. L. Zhang, W. Ma, H. Ade, O. Inganas, K. Gundogdu, F. Gao and H. Yan, *Nat. Energy*, 2016, **1**, 16089.
39 W. Zhao, S. Li, H. Yao, S. Zhang, Y. Zhang, B. Yang and J. Hou, *J. Am. Chem. Soc.*, 2017, **139**, 7148.
40 D. Baran, R. S. Ashraf, D. A. Hanifi, M. Abdelsamie, N. Gasparini, J. A. Rohr, S. Holliday, A. Wadsworth, S. Lockett, M. Neophytou, C. J. Emmott, J. Nelson,

C. J. Brabec, A. Amassian, A. Salleo, T. Kirchartz, J. R. Durrant and I. McCulloch, *Nat. Mater.*, 2017, **16**, 363.
41 Y. Yang, Z. G. Zhang, H. Bin, S. Chen, L. Gao, L. Xue, C. Yang and Y. Li, *J. Am. Chem. Soc.*, 2016, **138**, 15011.
42 Y. Lin, J. Wang, Z. G. Zhang, H. Bai, Y. Li, D. Zhu and X. Zhan, *Adv. Mater.*, 2015, **27**, 1170.
43 Y. Lin, Q. He, F. Zhao, L. Huo, J. Mai, X. Lu, C. J. Su, T. Li, J. Wang, J. Zhu, Y. Sun, C. Wang and X. Zhan, *J. Am. Chem. Soc.*, 2016, **138**, 2973.
44 S. Dai, F. Zhao, Q. Zhang, T. K. Lau, T. Li, K. Liu, Q. Ling, C. Wang, X. Lu, W. You and X. Zhan, *J. Am. Chem. Soc.*, 2017, **139**, 1336.
45 Y. Lin, F. Zhao, Q. He, L. Huo, Y. Wu, T. C. Parker, W. Ma, Y. Sun, C. Wang, D. Zhu, A. J. Heeger, S. R. Marder and X. Zhan, *J. Am. Chem. Soc.*, 2016, **138**, 4955.
46 Y. Z. Lin, Z. G. Zhang, H. T. Bai, J. Y. Wang, Y. H. Yao, Y. F. Li, D. B. Zhu and X. W. Zhan, *Energy Environ. Sci.*, 2015, **8**, 610.
47 H. Bin, Z. G. Zhang, L. Gao, S. Chen, L. Zhong, L. Xue, C. Yang and Y. Li, *J. Am. Chem. Soc.*, 2016, **138**, 4657.
48 N. Qiu, H. Zhang, X. Wan, C. Li, X. Ke, H. Feng, B. Kan, H. Zhang, Q. Zhang, Y. Lu and Y. Chen, *Adv. Mater.*, 2017, **29**, 1604964.
49 B. Kan, H. Feng, X. Wan, F. Liu, X. Ke, Y. Wang, Y. Wang, H. Zhang, C. Li, J. Hou and Y. Chen, *J. Am. Chem. Soc.*, 2017, **139**, 4929.
50 Z. G. Zhang, B. Y. Qi, Z. W. Jin, D. Chi, Z. Qi, Y. F. Li and J. Z. Wang, *Energy Environ. Sci.*, 2014, **7**, 1966.
51 P. W. M. Blom, V. D. Mihailetchi, L. J. A. Koster and D. E. Markov, *Adv. Mater.*, 2007, **19**, 1551.
52 C. M. Proctor, M. Kuik and T. Q. Nguyen, *Prog. Polym. Sci.*, 2013, **38**, 1941.

